European Geosciences Union General Assembly 2017, EGU
Division Energy, Resources & Environment, ERE

Hydrodynamic Impacts of a Marine Renewable Energy Installation on the Benthic Boundary Layer in a Tidal Channel

Shaun Fraser[a],*, Vladimir Nikora[a], Benjamin J. Williamson[b], Beth E. Scott[b]

aSchool of Engineering, University of Aberdeen, Aberdeen AB24 3UE, UK
bSchool of Biological Sciences, University of Aberdeen, Aberdeen AB24 2TZ, UK

Abstract

Field measurements of the flow in the benthic boundary layer (BBL) of a tidal channel are presented which compare data collected in the wake of a marine renewable energy installation (MREI) with control data representative of the natural conditions. The results show significant flow modification in the wake of the MREI including a reduction in mean velocity, enhanced turbulence, and the breakdown of the natural structure and dynamics of the BBL. This study provides new information relevant to the environmental impact assessment of MREIs and to the design and consenting of marine renewable energy projects.

© 2017 The Authors. Published by Elsevier Ltd.
Peer-review under responsibility of the scientific committee of the European Geosciences Union (EGU) General Assembly 2017 – Division Energy, Resources and the Environment (ERE).

Keywords: Hydrodynamic impact; marine renewable energy; benthic boundary layer; tidal channel; turbulence; ADV; wake dynamics

1. Introduction

In the last decade there have been significant advances in tidal stream technologies with various turbine designs tested and numerous marine renewable energy installations (MREIs) deployed at sites around the world [1]. MREIs are designed to be deployed in energetic environments with high tidal flows where the available energy resource is maximized. These environments are found in tidal channels, where the local coastline and bathymetry constrain the flow leading to increased mean flow velocities and enhanced kinetic energy [2]. Tidal channels currently considered

* Corresponding author.
  E-mail address: s.fraser@abdn.ac.uk

for industrial developments typically have peak spring flow velocities in excess of 2.5 m s^{-1} and water depths in the range 25 - 50 m [3]. These sites are characterized by high levels of turbulence over a range of scales with high temporal and spatial variability [4-6].

Friction with the seabed leads to the formation of the benthic boundary layer (BBL) in tidal flows which is substantially non-stationary [7]. Early observations of the BBL in tidal channels focused on characterizing the velocity profile and shear stress across different bed configurations to understand sediment transport mechanisms [8]. Following the discovery of bursting phenomena in laboratory experiments [9-10] it was recognized that the dynamics of the BBL in tidal channels can be controlled by large, intermittent, and well-organized motions [11]. Bursting motions generated in the BBL have also been shown to interact with stratification in tidal channels and surface wave dynamics [12]. Further, these processes can interact with the larger scale dynamics related to the coastline and bathymetry, for example vortex shedding from islands and large eddies in the wake of headlands [13–14]. Consequently, the natural dynamics of the BBL in tidal channels involves highly complex turbulence which presents a challenge for the survivability of tidal turbines [15] and the effectiveness of environmental monitoring technologies [16-17].

It is not yet clear how exactly the presence of MREIs will affect the natural characteristics of the BBL in tidal channels. A detailed understanding of the dynamics of the wake flow behind MREIs is essential for understanding the ecological impacts [18], the effects on physical processes [19], and for the design of device arrays for optimal power output [20]. Extensive numerical modelling work has been undertaken over recent years to investigate the wake dynamics of tidal stream turbines [21]. Further insights are available from various experimental studies using scaled model turbines in laboratory simulations [22] which have shown that wake characteristics are strongly dependent on the natural turbulence conditions [23]. The highly complex structure of turbulence in tidal channels makes field observations essential to validate models of wake flows and gain confidence in predictions relevant to the design and optimization of devices.

Most recent hydrodynamic measurements in tidal channels have been collected by moored acoustic Doppler current profiler (ADCP) deployments [5,24-25] which can have the advantage of depth coverage over most of the water column. However, the analysis of turbulence from ADCP data is limited as the instantaneous three-dimensional velocity cannot be reliably resolved due to the assumptions of horizontal homogeneity between beams. In contrast, an acoustic Doppler velocimeter (ADV) can provide reliable velocity measurements at high sampling rates and within a small sampling volume to obtain detailed information on the properties of turbulence relevant to understanding the dynamics of the BBL [26] and the nature of unsteady loading on tidal turbines [15]. Previous studies have utilized ADVs mounted several meters from the seabed in tidal channels to characterize the natural turbulence at turbine hub height [6,14,27]. However, ADV assessments of the BBL in tidal channels are lacking and there are very few hydrodynamic field observations from around full-scale MREIs due to the operational difficulties of data collection.

In this study, analysis of ADV data provides information on the mean flow and turbulence characteristics in the BBL of a tidal channel. Results from a control site representative of the natural conditions are compared to results from the wake of a tidal stream turbine foundation to provide essential information on the hydrodynamic impacts of MREIs.

2. Method

2.1. Study site

The data used in this study were collected at the Fall of Warness (FoW) tidal test site at the European Marine Energy Centre (EMEC), UK, during summer 2013. FoW is a tidal channel located in the Orkney Islands between the islands of Eday and Muckle Green Holm (59°7' to 59°11'N, 2°47' to 2°50'W) and is an energetic marine environment which is representative of the sites targeted for tidal stream energy extraction globally. FoW is characterized by semidiurnal tidal currents exceeding 3.5 m s^{-1} during peak spring tides. The principal semidiurnal lunar (M_2) and solar (S_2) tidal constituents dominate the dynamics of the site which is subject to strong tidal currents due to the interaction of the North Sea and North Atlantic [28]. The tides flow from the north-west to the south-east during the flood tidal phase, and from the south-east to the north-west during the ebb tidal phase.

2.2. Data collection

Data were collected during FLOWBEC (FLOW and Benthic Ecology project) platform deployments in 2013 [29]. A SonTek/YSI ADVOcean operating at 5 MHz was used to collect high-precision three-dimensional flow velocity data with a resolution of 0.1 cm s^{-1} and an accuracy of ± 1 % of the measured velocity. The ADV was set at a sampling rate of either 16 Hz or 20 Hz, recording for 25 minute bursts separated by five minutes. Each sample includes three instantaneous velocity components in Cartesian coordinates (u, v, w).

The ADV probe was mounted within a mooring frame and oriented facing upwards so that the ~2 cm^3 sampling volume was approximately 85 cm above the seabed and at approximately 34 m depth. The probe was positioned so that the flow through the sampling volume was unobstructed along the axis of tidal flow to minimize any interference from frame components as much as possible given practical limitations. The ADV was configured so that the v component of velocity was oriented approximately parallel with the tidal flow directions, the u component was therefore approximately transverse to the flow, and the w component was vertical. Flow in the ebb direction was approximately in the +v direction while the flood flow was approximately in the -v direction. The +w component of velocity was oriented vertically downward towards the bed, and the -w component of velocity was oriented vertically upwards.

Data from two platform deployments are considered in this study. The first platform deployment was from June 3rd - 15th and was positioned 15 m downstream (during flood) from the seabed installed Atlantis AK-1000 tidal turbine foundation (composed of a tripod base with three 4 m high ballast blocks and a 10 m high central piling) to provide the "MREI present" dataset. The second platform deployment was positioned nearby in the same site for recording control data out of the wake of any installations from June 18th - July 5th to provide the "Control" dataset. Analysis was focused over a flood-ebb cycle from each deployment selected to give the best comparison from available data considering spring-neap variations and meteorological conditions. The selected data provide a typical flood-ebb cycle for the two platform deployments occurring between spring and neap, with the tidal range above the platform observed to be approximately 1.5 m. The comparisons of the two selected 14 hour data sections (Table 1) are the focus of this study.

Table 1. Summary of selected ADV data.

Dataset	Distance from bed	Sampling frequency	Burst duration	Burst interval	Samples per burst	Bursts selected	Coverage of selected data
MREI present	85 cm	20 Hz	25 min	5 min	30 000	28	June 3rd - 4th
Control	85 cm	16 Hz	25 min	5 min	24 000	28	June 18th - 19th

2.3. Data processing and computation of turbulence characteristics

Data were inspected to ensure that signal correlation values were in excess of 70 % as required by the manufacturer's guidelines [30] indicating high quality velocity data. However, even in ideal operating conditions ADVs are susceptible to various sources of errors and noise which can compromise the quality of measurements [31-32]. In particular, aliasing of the Doppler signal can lead to spikes in the record which should be removed before analysis. Spikes were detected by the phase-space thresholding method [33] and replaced with a cubic polynomial fitted to 12 points on either side of the spike.

Statistical quantities were computed using five minute non-overlapping windows, and therefore five windows per burst. Five minutes was determined empirically to be the longest duration which was statistically stationary as longer windows require detrending and shorter windows tend to underestimate the variance of large scale turbulent motions [6]. Velocity data are described by a fluctuating (denoted by a prime) and mean component (denoted by an overbar) for each five minute window following the Reynolds decomposition $u = u' + \overline{u}$, $v = v' + \overline{v}$ and $w = w' + \overline{w}$. Further bulk statistics were obtained using standard formulae for u , v , and w to give standard deviation (σ), skewness, and kurtosis.

Turbulence characteristics were computed in a directionally invariant form to account for the natural variation in flow direction relative to the probe orientation. Turbulence kinetic energy is the energy per unit mass associated

with the turbulent fluctuating components of flow velocity and defined here as $TKE = 1/2(\overline{u'^2} + \overline{v'^2} + \overline{w'^2})$. Turbulent stresses are described by the Reynolds stress $RES = (\overline{u'w'}^2 + \overline{v'w'}^2)^{1/2}$ which characterizes the vertical transfer of momentum. The estimated RES can be used to evaluate the shear (or friction) velocity $v_f = (RES)^{1/2}$ which is the characteristic velocity scale that describes the hydraulic stresses. It is also useful to define the mean horizontal velocity $\overline{v_H} = (\overline{u}^2 + \overline{v}^2)^{1/2}\overline{v}/|\overline{v}|$ with associated instantaneous and fluctuating components which are assigned direction by the v component oriented along the approximate flow axis so that negative values correspond to flood and positive values correspond to ebb. The relative turbulence intensity $TI = (TKE)^{1/2}/|\overline{v_H}|$ quantifies the magnitude of velocity fluctuations with respect to the mean horizontal flow and is expressed here as a %.

Power spectral density (PSD) estimates are computed using an overlapping segment-averaging method with a Hamming smoothing window and 50 % segment overlap.

The correlation function R describes the strength of the correlation between two time series for a given time lag τ. The prevailing (integral) scales of velocity fluctuations are obtained from the autocorrelation of the horizontal velocity component $R_{v_H'v_H'}(\tau) = \overline{v_H'(t)v_H'(t+\tau)}/\sigma_{v_H}^2$ and the autocorrelation of the vertical velocity component $R_{w'w'}(\tau) = \overline{w'(t)w'(t+\tau)}/\sigma_{w'}^2$ as $I_{v_H'v_H'} = \int R_{v_H'v_H'}(\tau)d\tau$ and $I_{w'w'} = \int R_{w'w'}(\tau)d\tau$ where the autocorrelation functions are integrated between the limits $\tau = 0$ and the first instance where autocorrelation reaches zero, e.g., $\tau(R_{v_H'v_H'}(\tau) = 0)$. Spatial context is provided using Taylor's frozen turbulence hypothesis and the integral length scales $L_{v_H'v_H'} = \overline{v_H}I_{v_H'v_H'}$ and $L_{w'w'} = \overline{v_H}I_{w'w'}$.

The correlation between velocity components relates to the three-dimensional structure of turbulent motions and is characterized by the cross-correlation function $R_{v_H'w'}(\tau) = \overline{v_H'(t)w'(t+\tau)}/(\sigma_{v_H'} \cdot \sigma_{w'})$.

3. Results

3.1. Mean flow velocity

Instantaneous and mean flow velocity data for a flood-ebb cycle are presented (Fig. 1). Mean flow data show a clear semidiurnal tidal pattern at both the control site and in the presence of the MREI. In both cases, the v component of velocity is dominant and approximately oriented parallel to the flow axis. For all velocity components the magnitude of fluctuations scale with the magnitude of mean velocity and are greatest during peak flows. In both datasets, the first approximately six hours of the records relate to the flood phase and provide data on the wake flow in the presence of the MREI. The mean horizontal velocity accounts for differences in probe orientation and flow direction (visible as the difference in the sign of u component results) and suggests a slight flood dominance in the control and a clear reduction in the mean flow velocity associated with the MREI. Although ebb peak values of $\overline{v_H}$ are similar in the two datasets, there is a clear difference in flood peak values of $\overline{v_H}$, i.e., -122.9 cm s^{-1} in the control observations compared to -85.4 cm s^{-1} in the presence of the MREI corresponding to a 31 % velocity deficit behind the MREI.

3.2. Bulk turbulence characteristics

The first four moments of all three components of velocity show that bulk statistics are strongly linked to the mean horizontal velocity at the site (Fig. 2). Skewness and kurtosis variations are similar between deployments, with increased asymmetry and intermittency occurring during slack conditions. Trends for velocity standard deviation σ are similar between deployments; however, despite the substantially greater velocities recorded during the flood phase in the control, σ is highest during flood conditions in the presence of the MREI. This result suggests that the velocity deficit observed in the wake of the MREI is associated with comparatively high velocity fluctuations and enhanced turbulence.

Velocity fluctuations are investigated in more detail by comparing further turbulence characteristics (Fig. 3). Trends are again driven by the tidal pattern in mean horizontal velocity in the site. However, comparison of flood and ebb for each dataset indicates significant differences associated with flow direction. TKE in the control results is relatively balanced with peak ebb TKE reaching 762.2 cm^2 s^{-2} and peak flood TKE measured at 878.2 cm^2 s^{-2}. This slight increase may be expected in the natural flow due to the slight flood dominance of peak velocities. However, the data in the presence of the MREI demonstrate much greater directional differences. The ebb peak TKE is

comparable with the control at 622.4 cm^2 s^{-2} while the peak flood TKE measured in the wake of the MREI reaches 1234.2 cm^2 s^{-2}, much higher than the control results despite the significant decrease in mean velocity.
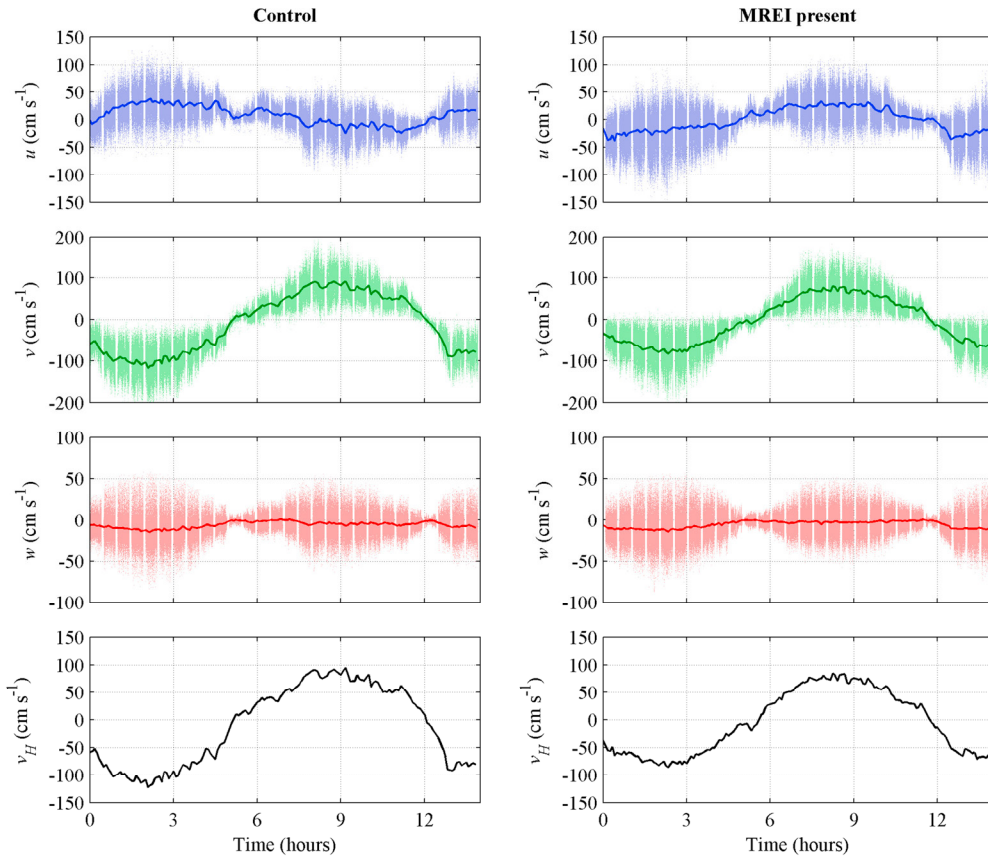

Fig. 1. Comparison of flow velocity data at a control site (left panels) and 15 m from a MREI (right panels) during a comparable flood-ebb cycle. Instantaneous values are shown by dots and mean values computed for five minute windows are shown by the solid lines. The flood phase corresponds to $-\overline{v_H}$ values which are recorded in the wake of a turbine foundation during MREI present results.

The analysis of RES and v_f indicates further differences between the datasets. In both the control and MREI presence, the ebb phase is dominant for RES and v_f. However, flood data in the wake of MREI are highly irregular and do not have the clear relation with flow velocity seen in the control. These results suggest some breakdown of the natural turbulence structure in the wake of the MREI related to increased TKE and reduced mean velocity.

The wake flow of the MREI is also characterized by a clear increase in TI which is approximately 10 % higher during flood than in ebb in the presence of the MREI. In contrast, TI in the control measurements is comparable in both flow directions suggesting that TI in the natural flow is balanced between the ebb and flood phases. In both cases, very high TI values are associated with slack conditions and division by near-zero $\left|\overline{v_H}\right|$.

TKE and TI can be plotted against the absolute mean horizontal velocity (Fig. 4) to further investigate the apparent increase in these turbulence characteristics observed in the wake of the MREI. These results provide striking evidence confirming that the flood measurements in the wake of the MREI are consistently characterized by elevated TKE and TI associated with a reduction in $\left|\overline{v_H}\right|$. At high flows, TI in the wake is up to almost 40 % which is a 10 – 15 % increase compared to the control results.
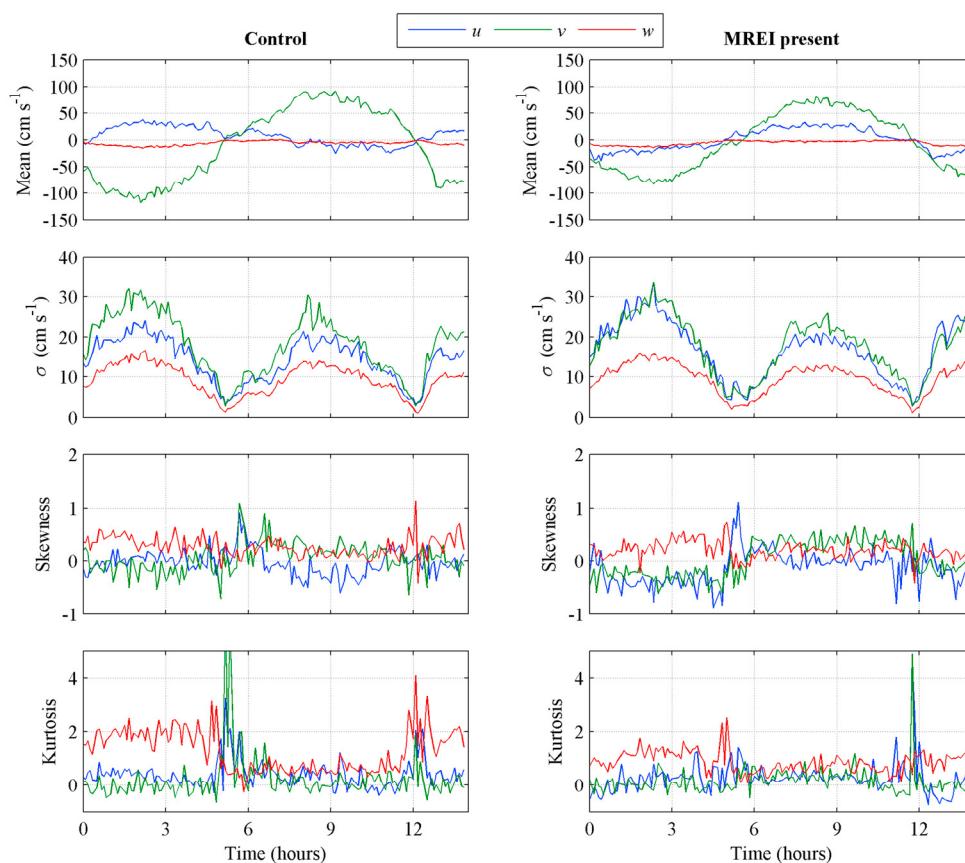
Fig. 2. Comparison of velocity bulk statistics results for a flood-ebb cycle. In each case, color corresponds to the velocity component. Mean, standard deviation (σ), skewness, and kurtosis are computed using five minute windows and standard formulae with a -3 correction applied to kurtosis.

3.3. Power spectra

The *PSD* results for the horizontal and vertical fluctuating velocity components during the ebb and flood phases are presented (Fig. 5). Spectra were computed using the average of 50 % overlapping five minute segments for the horizontal and vertical velocity components. In each case, the results are shown for the ADV burst during the observed peak flood and ebb flows in the selected data. The power spectra reveal the existence of well-established -1 and -5/3 frequency (f) scaling regions for horizontal velocity expected for high-Reynolds number wall-bounded turbulence [34]. Significantly higher *PSD* magnitudes for v_H compared to w at low-frequencies demonstrate anisotropy at larger scales consistent with boundary layer turbulence. At peak flows there are no clear differences in spectral characteristics which can be attributed to the flow direction, and there is no dominant spectral frequency component of the MREI wake.

3.4. Autocorrelation functions and integral scales

Autocorrelation functions and integral scales are also considered for five minute windows from the ADV bursts during the observed peak flood and ebb flows. Results are presented which provide information on the prevailing horizontal and vertical scales of turbulence (Fig. 6). The averaged autocorrelation functions are shown for each case and used to compute the integral time and length scales. As with the power spectra, the autocorrelation and integral scales for the different flow directions and deployments are generally comparable, with the horizontal scales dominant in all cases. However, $I_{w'w'}$ and the integral length scales calculated in the wake of MREI are less than in all other cases and in particular are reduced when compared against flood results at the control site.
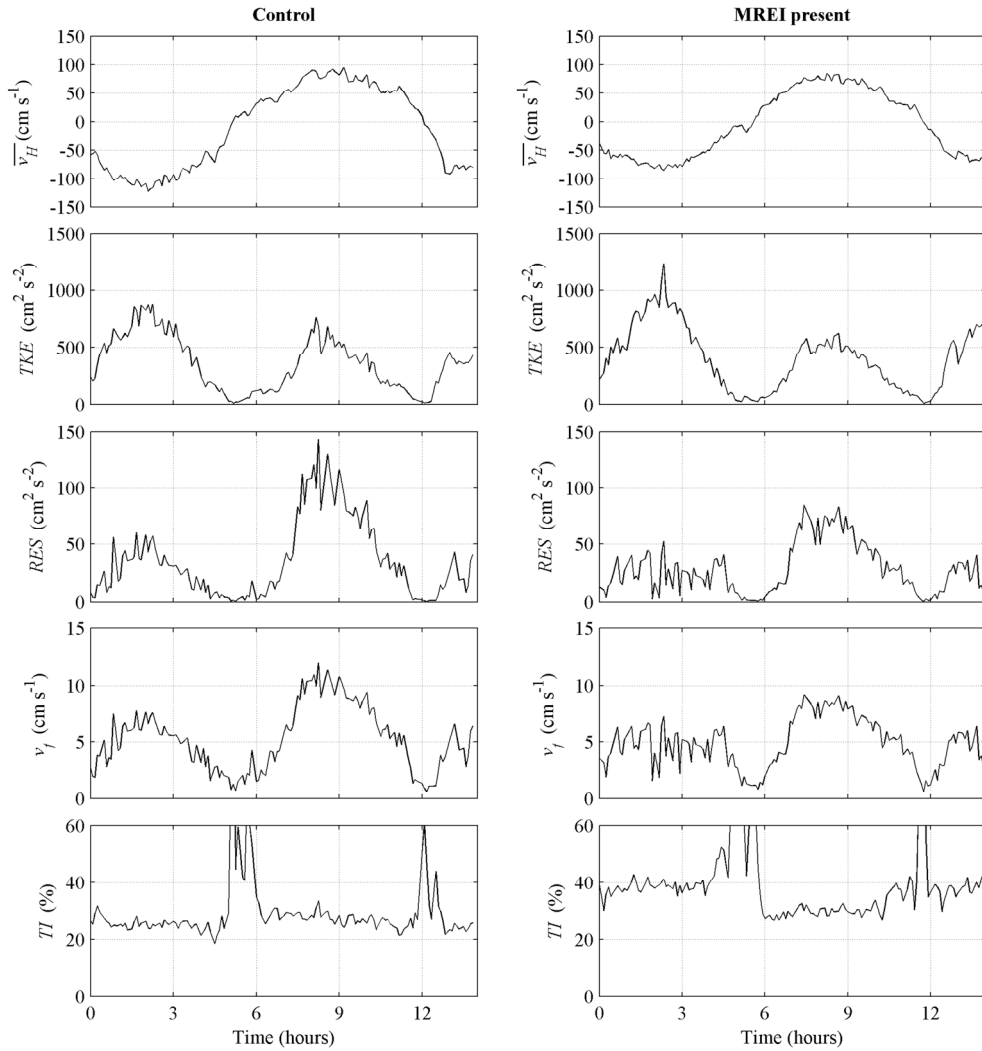
Fig. 3. Comparison of turbulence characteristics for a flood-ebb cycle. Mean horizontal velocity ($\overline{v_H}$), turbulence kinetic energy (TKE), Reynolds stress (RES), friction velocity (v_f), and relative turbulence intensity (TI) are computed using five minute windows.
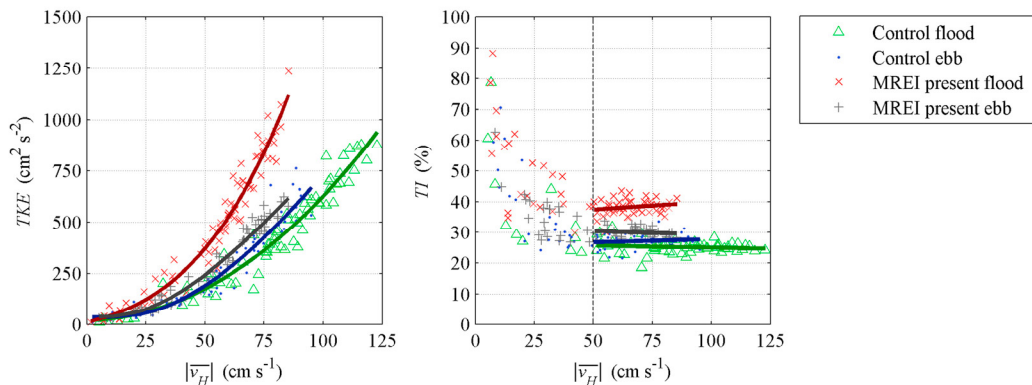

Fig. 4. Turbulence kinetic energy (TKE) and relative turbulence intensity (TI) plotted against the absolute mean horizontal velocity ($|\overline{v_H}|$). In both cases results are separated by dataset and by flow direction. A best fit polynomial is shown for TKE points, and a straight line fitted to TI points in excess of 50 cm s⁻¹.
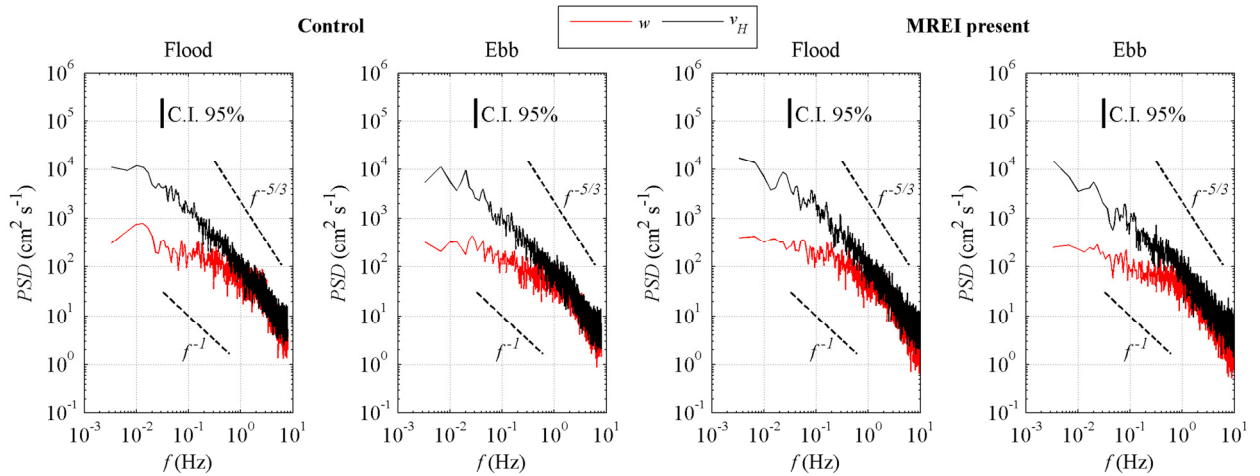
Fig. 5. Power spectral density (*PSD*) estimates for the horizontal and vertical velocity components with 95 % confidence intervals. Example slopes are shown for the well known $f^{-5/3}$ inertial subrange scaling law and the f^{-1} scaling law for boundary layer turbulence.
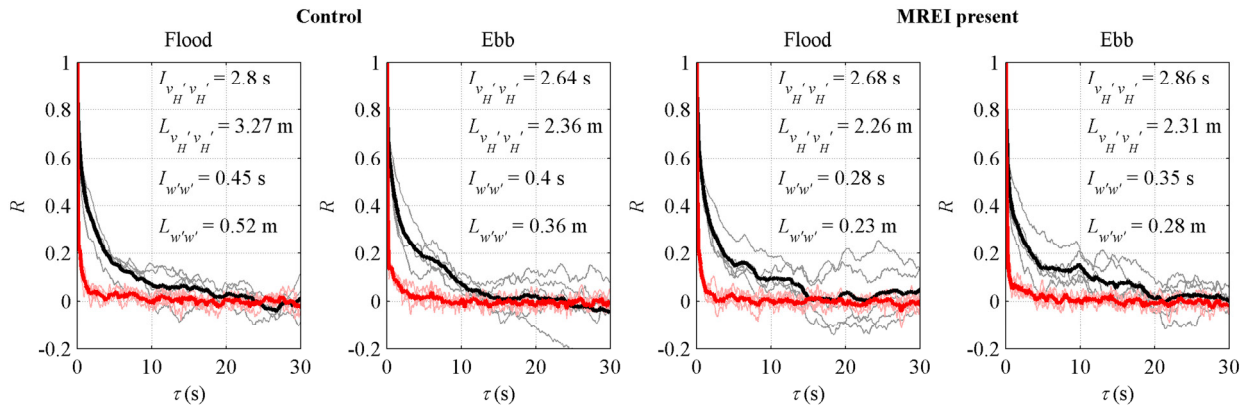

Fig. 6. Comparison of autocorrelation function results for v_H (shown in black) and w (shown in red) for peak flood and ebb flows. The thick line shows the average result for each case which is used to calculated the integral scales shown.

3.5. Cross-correlation functions

The relationship between horizontal and vertical velocity fluctuations is investigated using the cross-correlation functions (Fig. 7). As before, results are presented for five minute windows from the ADV bursts during the peak observed flood and ebb flows. The data at the control site demonstrate a strong correlation centered at $\tau = 0$ in both flood and ebb with the opposite sign corresponding to the change in direction of v_H. This implies that turbulent fluctuations in the flow direction are associated with downwards vertical motions in both the flood and ebb, providing evidence of the dominance of overturning coherent structures in the natural flow. The ebb results for the two deployments are similar as expected; however, there is a clear difference between flood results which suggests significant modification to the structure of turbulence in the wake of the MREI. The otherwise consistently observed relationship between velocity components is shown to break down in the wake flow, leaving a weak positive correlation at $\tau = 0$ during the flood in the presence of the MREI.
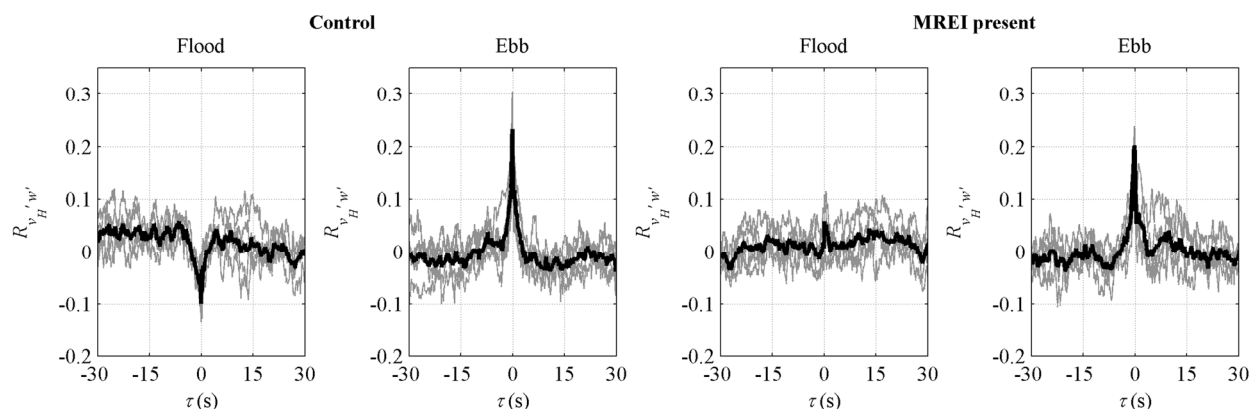
Fig. 7. Comparison of cross-correlation function for the vertical and horizontal components of velocity during peak flood and ebb flows. The thick line shows the average result for each case.

4. Conclusions

Field measurements of the flow in a tidal channel have revealed the hydrodynamic impact of a full-scale MREI. Velocity measurements 85 cm from the seabed were used to derive turbulence characteristics to quantify and interpret the dynamics of the BBL. Analysis focused on the comparison of a flood-ebb cycle recorded 15 m from a tidal stream turbine foundation and at a control site representative of the natural flow conditions.

Mean velocity results showed a clear reduction in peak mean velocity in the wake of the MREI corresponding to a 31 % velocity deficit compared to the control site. This reduced mean velocity was associated with comparatively high velocity fluctuations linked to systematic directional variations in turbulence characteristics. The wake flow was clearly linked to enhanced TKE and a 10 - 15 % increase in TI. Spectral characteristics were consistent with boundary layer turbulence and did not indicate a dominant spectral frequency of the MREI wake. However, the prevailing scales of turbulence were reduced during peak flow in the MREI wake. RES and v_f results suggested that the MREI wake was associated with the breakdown of the natural turbulence structure, with further evidence of modification to the three-dimensional structure of turbulence provided by the clear reduction in the cross-correlation of the vertical and horizontal velocity components.

The point measurements in this study proved to be useful for considering turbulence at fine-scales and the MREI wake dynamics in detail. However, to understand how the revealed effects vary spatially then an array of such measurements would be needed to provide information on the vertical and horizontal extents of the impacts. Further field observations are necessary to investigate the wake dynamics of operational marine energy devices of different designs.

This study provides information on the natural dynamics of the BBL in a tidal channel and much-needed insights into the hydrodynamic impacts of marine renewable energy developments near the bed. These results inform related observations of ecological impacts of MREIs [35], and provide evidence of the modified flow conditions that may be linked to changes in the behavior of mobile marine animals and benthic biota observed in such sites.

Acknowledgements

References

[1]   Zhou, Z., Benbouzid, M., Charpentier, J.F., Scuiller, F. and Tang, T., (2017). Developments in large marine current turbine technologies–A
      review. *Renew. Sustain. Energy Rev.*, 71, pp.852-858.

[2]   Bahaj, A.S., (2011). Generating electricity from the oceans. *Renew. Sustain. Energy Rev.*, 15(7), pp.3399-3416.
[3]   Lewis, M., Neill, S.P., Robins, P.E. and Hashemi, M.R., (2015). Resource assessment for future generations of tidal-stream energy arrays. *Energy*, 83, pp.403-415.
[4]   Lu, Y., Lueck, R.G. and Huang, D., (2000). Turbulence characteristics in a tidal channel. *J. Phys. Oceanogr.*, 30(5), pp.855-867.
[5]   Rippeth, T.P., Williams, E. and Simpson, J.H., (2002). Reynolds stress and turbulent energy production in a tidal channel. *J. Phys. Oceanogr.*, 32(4), pp.1242-1251.
[6]   Thomson, J., Polagye, B., Durgesh, V. and Richmond, M.C., (2012). Measurements of turbulence at two tidal energy sites in Puget Sound, WA. *IEEE J. Oceanic Eng.,* 37(3), pp.363-374.
[7]   Monin, A.S. and Ozmidov R.V., (1985). *Turbulence in the Ocean*. Dordrecht, Holland, Reidel.
[8]   Sternberg, R.W., (1968). Friction factors in tidal channels with differing bed roughness. *Mar. Geol.*, 6(3), pp.243-260.
[9]   Kline, S.J., Reynolds, W.C., Schraub, F.A. and Runstadler, P.W., (1967). The structure of turbulent boundary layers. *J. Fluid Mech.*, 30(04), pp.741-773.
[10] Corino, E.R. and Brodkey, R.S., (1969). A visual investigation of the wall region in turbulent flow. *J. Fluid Mech.*, 37(01), pp.1-30.
[11] Heathershaw, A.D., (1979). The turbulent structure of the bottom boundary layer in a tidal current. *Geophys. J. Int.*, 58(2), pp.395-430.
[12] Thorpe, S.A., Green, J.A.M., Simpson, J.H., Osborn, T.R. and Nimmo Smith, W.A.M., (2008). Boils and turbulence in a weakly stratified shallow tidal sea. *J. Phys. Oceanogr.*, 38, 1711–1730.
[13] Signell, R.P. and Geyer, W.R., (1991). Transient eddy formation around headlands. *J. Geophys. Res.*, 96(C2), pp.2561-2575.
[14] McCaffrey, K., Fox-Kemper, B., Hamlington, P.E. and Thomson, J., (2015). Characterization of turbulence anisotropy, coherence, and intermittency at a prospective tidal energy site: Observational data analysis. *Renew. Energy*, 76, pp.441-453.
[15] Milne, I.A., Day, A.H., Sharma, R.N. and Flay, R.G.J., (2016). The characterisation of the hydrodynamic loads on tidal turbines due to turbulence. *Renew. Sustain. Energy Rev.*, 56, pp.851-864.
[16] Melvin, G.D. and Cochrane, N.A., (2015). Multibeam acoustic detection of fish and water column targets at high-flow sites. *Estuar. Coast.,* 38(1), pp.227-240.
[17] Fraser, S., Nikora, V., Williamson, B.J. and Scott, B.E., (2017). Automatic active acoustic target detection in turbulent aquatic environments. *Limnol. Oceanogr. Methods*, 15(2), pp.184-199.
[18] Shields, M.A., Woolf, D.K., Grist, E.P., Kerr, S.A., Jackson, A.C., Harris, R.E., Bell, M.C., Beharie, R., Want, A., Osalusi, E. and Gibb, S.W., (2011). Marine renewable energy: The ecological implications of altering the hydrodynamics of the marine environment. *Ocean Coast. Manage.*, 54(1), pp.2-9.
[19] Robins, P.E., Neill, S.P. and Lewis, M.J., (2014). Impact of tidal-stream arrays in relation to the natural variability of sedimentary processes. *Renew. Energy*, 72, pp.311-321.
[20] Bai, G., Li, J., Fan, P. and Li, G., (2013). Numerical investigations of the effects of different arrays on power extractions of horizontal axis tidal current turbines. *Renew. Energy*, 53, pp.180-186.
[21] Lam, W.H., Chen, L. and Hashim, R., (2015). Analytical wake model of tidal current turbine. *Energy*, 79, pp.512-521.
[22] Morandi, B., Di Felice, F., Costanzo, M., Romano, G.P., Dhomé, D. and Allo, J.C., (2016). Experimental investigation of the near wake of a horizontal axis tidal current turbine. *Int. J. Mar. Energy*, 14, pp.229-247.
[23] Mycek, P., Gaurier, B., Germain, G., Pinon, G. and Rivoalen, E., (2014). Experimental study of the turbulence intensity effects on marine current turbines behaviour. Part I: One single turbine. *Renew. Energy*, 66, pp.729-746.
[24] Lu, Y. and Lueck, R.G., (1999). Using a broadband ADCP in a tidal channel. Part I: Mean flow and shear. *J. Atmos. Oceanic Technol.*, 16(11), pp.1556-1567.
[25] Osalusi, E., Side, J. and Harris, R., (2009). Structure of turbulent flow in EMEC's tidal energy test site. *Int. Commun. Heat Mass Transf.*, 36(5), pp.422-431.
[26] Nikora, V., Goring, D. and Ross, A., (2002). The structure and dynamics of the thin near-bed layer in a complex marine environment: a case study in Beatrix Bay, New Zealand. *Estuar. Coast. Shelf Sci.*, 54(5), pp.915-926.
[27] Milne, I.A., Sharma, R.N., Flay, R.G. and Bickerton, S., (2013). Characteristics of the turbulence in the flow at a tidal stream power site. *Phil. Trans. R. Soc. A.*, 371, 20120196.
[28] Neill, S.P., Hashemi, M.R. and Lewis, M.J., (2014). The role of tidal asymmetry in characterizing the tidal energy resource of Orkney. *Renew. Energy*, 68, pp.337-350.
[29] Williamson, B.J., Blondel, P., Armstrong, E., Bell, P.S., Hall, C., Waggitt, J.J. and Scott, B.E., (2016). A self-contained subsea platform for acoustic monitoring of the environment around Marine Renewable Energy Devices–Field deployments at wave and tidal energy sites in Orkney, Scotland. *IEEE J. Oceanic Eng.*, 41(1), pp.67-81.
[30] SonTek, (2001). Acoustic Doppler Velocimeter Principles of Operation. SonTek/YSI Inc., pp.14.
[31] Nikora, V.I. and Goring, D.G., (1998). ADV measurements of turbulence: Can we improve their interpretation? *J. Hydraul. Eng.*, 124(6), pp.630-634.
[32] Voulgaris, G. and Trowbridge, J.H., (1998). Evaluation of the acoustic Doppler velocimeter (ADV) for turbulence measurements. *J. Atmos. Oceanic Technol.*, 15(1), pp.272-289.
[33] Goring, D.G. and Nikora, V.I., (2002). Despiking acoustic Doppler velocimeter data. *J. Hydraul. Eng.*, 128(1), pp.117-126.
[34] Nikora, V., (1999). Origin of the "− 1" spectral law in wall-bounded turbulence. *Phys. Rev. Lett.*, 83(4), p.734.
[35] Fraser, S., Williamson, B.J., Nikora, V. and Scott, B.E., (in review). Fish distributions in a tidal channel reveal the behavioural impact of a marine renewable energy installation. *Biol. Lett.*